Recent Progress in the Use of Perovskites for Electrochemical, Photoelectrochemical, and Photovoltaic–Electrochemical CO$_2$ Reduction

Mina Ahmadi-Kashani [1] , **Mahmoud Zendehdel** [2,3,*], **Luigi Schirone** [4] , **Mohammad Mahdi Abolhasani** [1]
and **Narges Yaghoobi Nia** [4,5,*]

1   Chemical Engineering Department, University of Kashan, Kashan 8731753153, Iran;
    ahmadimina133@gmail.com (M.A.-K.); meh.abolhasani@gmail.com (M.M.A.)
2   Kimia Solar Research Institute (K.S.R.I), Kimia Solar Company, Kashan 8713745868, Iran
3   Iritaly Trading Company S.r.l., Via Volturno 58, 00185 Rome, Italy
4   School of Aerospace Engineering, Sapienza University of Rome, Via Salaria 851, 00138 Rome, Italy;
    luigi.schirone@uniroma1.it
5   Department of Electronics Engineering, University of Rome Tor Vergata, Via del Politecnico 1,
    00133 Roma, Italy
*   Correspondence: m.zendehdel@iritalytrading.com (M.Z.); narges.yaghoobinia@uniroma1.it (N.Y.N.)

Abstract: Developing novel functional materials to advance the technological level of clean and renewable energy systems is the focus of much research. Due to their outstanding operational and compositional properties, perovskite-based structures have already been studied as an important class of solid-state components for electrochemical (EC), photoelectrochemical (PEC), and photovoltaic–electrochemical (PV-EC) CO$_2$ reduction, showing great potential in their catalytic activity and device stability and with a promising window for further technological developments. In this review, the different kinds of perovskites in the context of their structural features, which lead to their different applications, are first investigated. Then, we summarize the recent progress in the use of perovskites in EC, PEC, and PV-EC CO$_2$-reduction devices. The research demonstrates that the mechanism and kinetics of intermediate formation have a significant effect on the creation of the final product. Investigations show that appropriate surface modifications, such as through the use of doping agents, alloy construction, and composites, can considerably improve the electrocatalytic activity and stability of perovskites. Finally, the perspectives on, and limitations of, the commercial and large-scale production of perovskites for CO$_2$ reduction are stated.

Keywords: perovskite; electrochemical; photoelectrochemical; photovoltaic–electrochemical; CO$_2$ reduction

1. Introduction

Anthropogenic CO$_2$ emissions have increased significantly as a result of the extensive use of fossil fuels for energy generation. The International Energy Agency estimates that around 81% of the world's energy consumption is met by fossil fuels. The entire energy demand is anticipated to increase to 24–26 TW by 2040, with CO$_2$ emissions averaging 37–44 Gt annually [1]. It is critical to close the carbon cycle because this is one of the biggest issues facing our civilization. Global warming, glacier melting, and ocean acidification are just a few of the environmental issues brought on by an excessive amount of CO$_2$ in the atmosphere. These issues have a long-term negative impact on both humans' wellbeing and the health of the planet's ecosystem [2,3]. As a result of these serious problems, developing progressive technologies for CO$_2$ capture, utilization, and storage (CCUS) is becoming increasingly necessary in the twenty-first century. Accordingly, we need to focus more on renewable energy sources and relevant transition technologies. Renewable energy systems such as solar and wind power can be considered the main sources of electricity supply,

and the rates of electrical energy produced from them is estimated to be comparable to conventional coal generation [4,5]. As essential operational resources for the exploitation and storing of renewable energy, electrocatalytic carbon dioxide reduction reactions can be performed to capture and activate stable CO_2 molecules via electrochemical (EC), photovoltaic–electrochemical (PV-EC), or photoelectrochemical (PEC) catalysis, resulting in the creation of a number of products such as methane, methanol, ethanol, carbon monoxide, formic acid, and so on [6,7]. Electrocatalysis is a catalytic process that involves the conversion of electrical energy into chemical energy through the use of electricity [8]. PV-EC consists of an integration between photovoltaic (PV) and electrochemical (EC) systems due to the capture of the incident photon and the use of the generated photovoltage for synthesizing the necessary carbon-based chemicals when fed with CO_2. Meanwhile, the photoelectrochemical (PEC) technique, which uses a semiconductor light collector and is integrated with an electrochemical catalyst in a device stack, is an outstanding method for CO_2 reduction, using sunlight as an energy supply [9,10]. Compared with conventional high-temperature thermal conversion, electrochemical CO_2 reduction using sustainable energy sources is more favorable because of its mild functional situations [11]. Electro-CO_2 reduction (CO_2ER) offers an attractive way to convert CO_2 into additional chemicals under standard ambient atmospheric temperature and pressure (SATP) conditions, and it can be simply joined with renewable energy sources like wind and solar power, providing a "green" path to carbon recycling [12]. However, because of the slow reaction mechanism of inert CO_2 molecules, which initiates a competitive process (hydrogen evolution reaction; HER) and leads to low faradaic efficiency in aqueous solutions, the practical application of direct CO_2ER has been seriously delayed [13]. In addition, due to the multiple proton–electron transfer mechanisms, CO_2ER products are usually very complex, leading to excessive costs for separation and purification [14].

As for CO_2ER, while many metallic (e.g., Ag, Au, Pd, Cu, Co, Sn) and non-metallic (e.g., N-doped graphene, carbon nanotubes) catalysts have been investigated and shown to have significant catalytic activity, their performance is much lower than expected [15]. For example, Sn derivatives have received a lot of attention because of the selectivity of their formed products, but they usually suffer from limited reaction selectivity and activity [13]. Therefore, using efficient catalysts with selectivity and acceptable activity is important but also challenging.

In recent decades, perovskites with the general formula ABX_3 have been devoted significant consideration owing to their flexible compositions and diverse properties, and they have found broad applications in the fields of electronics, photonics, photovoltaics, magnetism, and catalysis [16–21], showing a promising potential to reach the best sustainable solution based on the results of their life-cycle assessment (LCA) [22]. Previous studies have shown that the metal–oxygen bonds in the perovskite form the basis for the regulation of its electronic properties, which further affects the surface binding energy [23]. In addition, B (BO_5) surface sites with an asymmetric coordination environment also induce special surface properties for perovskites. The high flexibility in the arrangement and crystal structure of perovskites lead to their tunable electronic structure, with well-defined physical and chemical properties, making them ideal candidates as electrocatalysts for CO_2 reduction [24,25].

A review focusing on the application of perovskites in EC, PEC, and PV-EC for CO_2 reduction is still lacking, and a better understanding of recent advances in this important research area is essential. Here we focus on perovskites as electrocatalysts and provide an overview of their applications in CO_2 reduction.

2. Structure of Perovskites

Depending on their ability to occupy different cationic and anionic sites, perovskites can present in various forms, including as oxides, sulfides, nitrides, and metal–halides [26]. Perovskites have four dimensionalities, namely 0-D, 1-D, 2-D, and 3-D, which exist in various forms; for example, (a) ABX_3 perovskites (e.g., $CH_3NH_3PbI_3$, $CaTiO_3$), (b) A_2BX_4

layered perovskites (e.g., Cs_2PbI_4), (c) $A_2BB'X_6$ double perovskites (e.g., Sr_2FeMoO_6, Ba_2TiRuO_6), and (d) $A_2A'B_2B'X_9$ triple perovskites (e.g., $La_2SrCo_2FeO_9$) [27]. A variety of cation/anion combinations can be employed to create different shapes while maintaining charge neutrality.

2.1. Perovskite Oxides

Several transition metal oxides with the basic chemical formula of ABO_3 belong to the perovskite oxide family, where the 12-fold O-coordinated A-sites and the 6-fold O-coordinated B-sites are occupied by the larger alkali metals or rare-earth cations and the smaller transition metal cations, respectively. The A- and B-sites of perovskite oxides could be substituted by almost 90% of the elements in the periodic table. A common approach to expanding the perovskite family and adjusting its properties is doping new cations at A and B sites that possibly will lead to a random or well-organized arrangement. These oxides typically are in a cubic structure, but it is possible to display transitions to hexagonal, tetrahedral, orthorhombic, and rhombohedral structures [28]. Structural variations in perovskite oxides can lead to the realization of different magnetic orderings [29]. The appropriate substitution of anions/cations or the doping of these perovskites can create a variety of piezoelectric, ferroelectric, superconducting, catalytic, metallic, and magnetic properties [30]. This wide range of properties allows perovskite oxides to be used in various electronic devices, piezoelectric devices, biosensors, transducers, and actuators [31–33]. Owing to their structure flexibility, high stability, distinctive arrangement, ionic conductivity, as well as their electron mobility and redox behavior, perovskite oxides are also used as electrocatalysts in different reactions. In particular, the application of these perovskites in electrocatalysis have following advantages: (1) more stoichiometric regulation and homogeneity are provided at a low cost and in an easy synthetic procedure; (2) modulation of perovskite oxide properties lead to the use of a wide range of substituting components. Despite the extensive use of perovskite oxides in various fields, these compounds face serious challenges. For example, at high temperature, perovskite oxides can easily decompose or react with other materials. This can limit their use in high-temperature processes. In addition, some perovskite oxides contain toxic elements, which can affect human health and the environment. Another problem is that perovskite oxides in thin films have a tendency to form defects, which can affect their electronic and optical properties. Also, the deposition of a perovskite oxide thin film can be challenging, demanding the defined control of temperature, pressure, and other parameters to achieve the desired properties. One solution to addressing perovskite oxides is to modify the composition of these materials by introducing dopants or by changing the synthesis conditions. For example, adding small amounts of elements such as strontium or magnesium can improve the stability of perovskite oxides. Moreover, safer and more eco-friendly perovskite oxides are obtained using non-toxic elements [28].

2.2. Metal–Halide Perovskites

Owing to their favorable features such as efficient optoelectronic properties, low cost, and simple synthesis method, metal–halide perovskites can be considered a notable material for next-generation devices [34–36]. Metal–halide perovskites have a general formula of ABX3, where A is a monovalent organic or inorganic cation (e.g., $CH_3NH_3^+$, Cs^+), B is a divalent metal cation (e.g., Pb^{2+}), and X is a halide ion. Depending on the cations in the A-site of the perovskite structure, these compounds are divided into organometallic halide perovskites (OHPs) and inorganic halide perovskites (IHPs) [37–42]. Metal–halide perovskites display high absorption coefficients and high exciton emission and tunable energy bands at ambient temperature. Also, these perovskites are described as favorite direct-bandgap semiconductor compounds [43,44]. $MAPbI_3$ and $FAPbI_3$ are the main types of these perovskites and are the most widely applied materials in photovoltaic applications due to their high absorption coefficient and high electron and hole mobility [45]. In particular, these classes of hybrid metal–halide perovskites are well developed for various

scalable solution-based deposition techniques, with a promising pathway toward the sustainable generation of renewable energies [16,46–50]. In spite of their outstanding features, the metal–halide perovskites have serious problems in practical applications because of their lack of stability. For example, these materials are very sensitive to water vapor and oxygen. Halide perovskites encounter excessive challenges in their preparation and device operations because, in most polar solvents, they dissolve or even decompose as a result of their intrinsic ionic bond properties and low lattice energies. Moreover, some metal–halide perovskites comprise toxic elements, which can cause health and environmental risks. For example, lead-based halide perovskites have been found to be toxic, and they can cause neurological damage and other health problems. Discovering novel protective layers or ligands is crucial for stability purposes. Furthermore, there are many investigations to develop alternative, non-toxic halide perovskites to improve their performance. Other halide perovskites, such as those made with tin or bismuth, may be less toxic than lead-based perovskites [51].

3. Fundamentals of CO_2 Reduction

The electrochemical reduction of CO_2 is a promising and outstanding method that leads to diminishing greenhouse gas emissions by allowing renewable energy storage in different chemical forms. This procedure presents exceptional benefits; for instance, the EC method can employ some environmentally friendly energy sources like solar energy, and it can be carried out at atmospheric temperature and pressure. Meanwhile, through altering the electrolyte and applied voltage, the reaction conditions and products can be controlled [52]. Nevertheless, CO_2 is a stable and inert linear molecule that requires an appropriate electrocatalyst to assist in breaking the C=O bond. The EC process can yield a diversity of products, including formic acid, formate, oxalic acid or oxalate, carbon monoxide, formaldehyde, methanol, methane, ethanol, ethylene, and other products. Solid-oxide fuel cells (SOFCs) and organic- or inorganic-materials-based electrodes collected with typical electrochemical cells are usually utilized for CO_2 conversion in high-temperature and low-temperature methods, respectively.

SOFC systems reveal a higher selectivity, whereas low-temperature CO_2-reduction reactions usually provide a wide range of products. In addition, low-temperature CO_2-reduction systems involve large overpotentials and, thus, great power requests. In electrochemical CO_2RR, two, four, six, or eight electrons can be transferred. Table 1 displays the resultant thermodynamic electrochemical half-reactions of CO_2RR, the number of electrons involved in the reaction, and the related standard potentials of electrodes (versus a standard hydrogen electrode, SHE) [53].

Table 1. Different products obtained under the standard potentials of CO_2RR (versus a standard hydrogen electrode, SHE) at 1.0 atm and 25 °C.

Electrochemical Thermodynamic Half-Reactions	Standard Potentials (V) vs. SHE
$CO_2(g) + 4H^+ + 4e^- = C(s) + 2 H_2O(l)$	0.210
$CO_2(g) + 2H^+ + 2e^- = HCOOH(l)$	−0.250
$CO_2(g) + 2H^+ + 2e^- = CO(g) + H_2O(l)$	−0.106
$CO_2(g) + 4H^+ + 4e^- = CH_2O(l) + H_2O(l)$	−0.070
$CO_2(g) + 6H^+ + 6e^- = CH_3OH(l) + H_2O(l)$	0.016
$CO_2(g) + 8H^+ + 8e^- = CH_4(g) + 2H_2O(l)$	0.169
$2CO_2(g) + 2H^+ + 2e^- = H_2C_2O_4(aq)$	−0.500
$2CO_2(g) + 12H^+ + 12e^- = CH_2CH_2(g) + 4H_2O(l)$	0.064

Nowadays, in order to reduce the disadvantages and promote the benefits of electrochemical and photocatalytic techniques for efficient CO_2 reduction, the combination of both technologies is being investigated. In the photoelectrochemical technique (PEC), which is also known as artificial photosynthesis because it imitates nature's energy cycle, CO_2 reduces into various products at ambient pressure and temperature by harvesting

light energy. The PEC CO_2 reduction offers many advantages such as environmental compatibility, great selectivity, economic viability, and the use of solar as a renewable energy source. In PEC systems, photocathodes and anodes are p-type and n-type semiconductors, respectively. Whenever light is illuminated, electrons are formed at the conduction band (CB) and holes are generated at the valence band (VB), leading to band bending at the connection point of the p-type and n-type electrodes. To improve the CO_2 reduction efficiency, band bending is crucial to create discrete electrons and holes at the electrodes and the electrolyte interface [9]. In the PEC CO_2RR process in aqueous solution (pH = 7), various intermediates are produced. The reactions below show the creation of electrons and protons that lead to the formation of various products [54].

$$2H_2O(l) \rightarrow O_2(g) + 4H^+(aq) + 4e^- \quad E^\circ_{OX}{}^\circ = -1.23 \text{ V} \tag{1}$$

$$CO_2(aq) + e^- \rightarrow CO_2^-(aq) \; E^\circ_{red} = -1.65 \text{ V} \tag{2}$$
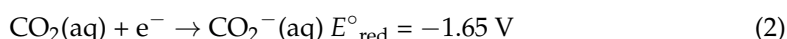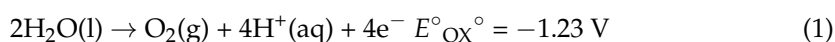
Reaction of water and holes:

$$H_2O + h^+ \rightarrow {}^\bullet OH + H^+ \tag{3}$$

$$2H_2O + 2h^+ \rightarrow H_2O_2 + 2H^+ \tag{4}$$

$$2H_2O + 4h^+ \rightarrow 4H^+ + O_2 \tag{5}$$

Formation of hydrogen radicals:

$$H^+ + e^- \rightarrow {}^\bullet H \tag{6}$$

Construction of CO_2 anion radicals:

$$CO_2 + e^- \rightarrow {}^\bullet CO_2^- \; E^\circ = -1.9 \text{ V} \tag{7}$$
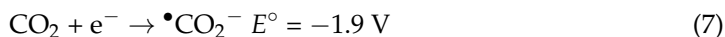
In the photoelectrochemical procedure, CO_2 can be transformed into different products, such as formaldehyde, carbon monoxide, formic acid, methane, methanol, ethanol, isopropanol, etc.

CO_2 reduction by using the solar system as a plentiful energy resource is considered a promising method to respond to the improvement in renewable energy sources aimed at sustaining human development amid increasing populations and the increasing demand for energy consumption. The combination of photovoltaic (PV) technology and electrochemical (EC) constituents delivers a route for transforming solar-energy-driven CO_2 into various beneficial chemicals and fuels. Furthermore, the applied potential for the development of $CO_2^{\bullet-}$ as an intermediate in CO_2 conversion is around -1.90 V (vs. NHE pH = 7.0), offering great overpotential for CO_2RR. Thus, applying PV-EC systems can provide sufficient energy for the conversion of CO_2 and create valued energy sources. Additionally, to achieve the highest activity, the PV modules and EC systems can be individually adjusted. PV systems can be connected to EC cells in parallel or series modes to achieve a supreme current density. For PV-EC systems, several solar cells, such as group III-V material, perovskite cells, Si, and dye-sensitized solar cells (DSSC), have been examined for CO_2RR [55].

4. Perovskites for CO_2 Reduction

Because of some exceptional features such as flexibility and high stability, as well as the ability to incorporate with a wide range of doping elements and substituting to control their properties, perovskites have attracted much attention for EC, PEC, and PV-EC applications. In this section, we summarize recent results of perovskite applications in EC, PEC, and PV-EC CO_2 reduction.

4.1. Direct Electrochemical CO$_2$ Reduction

An active and selective CO$_2$ reduction reaction (CO$_2$RR) is an important step in recycling excess CO$_2$ into renewable forms of carbon and building an energy-efficient society. Direct electrochemical CO$_2$RRs can proceed under ambient conditions and have been extensively studied to understand the fundamentals of catalysis and to develop efficient catalysts for practical applications [56]. Li et al. showed, for the first time, that a Sr$_2$Fe$_{1.5}$Mo$_{0.5}$O$_{6-\delta}$ (SFM) ceramic fuel-reforming electrode with a cubic perovskite structure can be used as an electrocatalyst to electrolyze pure CO$_2$ and convert it into CO without using syn-gases such as H$_2$ and CO in solid-oxide electrolysis cells [57]. Higher electrochemical efficiencies are demonstrated for single SFM cathodes using pure CO$_2$ as the feed gas compared with those reported for simple oxide–ceramic electrodes. The electrocatalytic properties of the SFM cathode for CO$_2$RR in solid-oxide electrolysis cells were tested by supported cells based on the double-layer electrolyte, containing an LSGM (La$_{0.9}$Sr$_{0.1}$Ga$_{0.8}$Mg$_{0.2}$O$_{3-\delta}$) electrolyte and an LDC (La$_{0.4}$Ce$_{0.6}$O$_{2-\delta}$) barrier layer with a thickness of ~230 μm and 5 μm, respectively. Owing to the improved conductivity and greater electrocatalytic activity at raised temperatures, higher current densities and faster CO$_2$RR rates were obtained by increasing the operational temperature. Applied temperatures of 650, 700, 750, and 800 °C under a voltage of 1.5 V led to current densities of 0.26, 0.33, 0.49, and 0.71 A·cm^{-2}, respectively. The achieved current density of 0.71 A·cm^{-2} was greater than almost all of the reported results for electrolyzing CO$_2$ using stable oxide electrodes at 800 °C. For CO$_2$ electrolysis under harsh conditions of pure CO$_2$ without a shielding gas, a relatively stable efficiency was obtained, and the current density reached above 1 A cm^{-2}; furthermore, the faradaic efficiency (FE) was above 95%, which was hardly ever attained in the literature but very desirable for commercial use. By using a SFM−Sm$_{0.2}$Ce$_{0.8}$O$_{2-\delta}$ composite cathode in 1.5 V and different temperatures of 650, 700, 750, and 800 °C, current densities of 0.40, 0.54, 0.75, and 1.09 A cm^{-2} were attained, respectively. Using the SFM−Sm$_{0.2}$Ce$_{0.8}$O$_{2-\delta}$ composite cathode, the electrocatalytic activity was considerably developed, and the current density showed a growth of about 53.5% in a practical voltage of 1.5 V at 800 °C. These results signified that the SFM ceramics are favorable catalysts for CO$_2$ electroreduction. Also, the dependence of the current density on various applied voltages versus time was investigated. The results showed that with an increase in applied voltage from 1.0 to 1.6 V, the CO creation ratio improved from 3.62 to 9.01 mL min^{-1} cm^{-2} with an FE$_{CO}$ of 95%. At a potential of 1.5 V, the potentiostatic analysis was directed for over 100 h, and after 8 h, only a small reduction in current density was observed.

SrSnO$_3$ nanowires (NWs) with a single 1D nanostructure and cubic perovskite phase have been reported by Pi et al. [58]. An adapted setup of a gas-tight two-chamber with a proton-exchange membrane (PEM) as the separator was designed for electrochemical investigation. An Ag/AgCl electrode, carbon-fiber-paper-modified SrSnO$_3$ nanowires in the cathodic chamber, and a Pt wire in the anodic chamber were used as the reference electrode (RE), working electrode (WE), and counter electrode (CE), respectively. When applied to CO$_2$ER catalysis, these prepared perovskite NWs show outstanding selectivity and catalytic activity in formate production, with a high FE (~80%) and remarkable current density over a wide potential range, making them outstanding electrocatalysts for the CO$_2$ electroreduction to formate. Consequently, great selectivity (~80%), a large current density (21.6 mA cm^{-2}), and a notable durability of at least 10 h were obtained, making a new class of perovskite NWs with potential applications for CO$_2$ER and beyond. In comparison, bulk SrSnO$_3$ and SnO$_2$ nanoparticles (NPs) show very low activity and/or selectivity for CO$_2$ER. Further analysis shows that the SrSnO$_3$ NWs have optimized efficient CO$_2^{\bullet-}$ stabilization and slow hydrogen evolution reaction (HER) kinetics, all of which contribute to the effective reduction of CO$_2$ to formate. The theoretical experiments proposed that the formation of CO$_2^{\bullet-}$ was the rate-determining step (RDS) for CO$_2$ reduction on the SrSnO$_3$ NW catalysts. Indeed, stabilization of CO$_2^{\bullet-}$ had a main role in CO$_2$ reduction in supporting the kinetics for the production of formate and in reducing the reaction obstacles. Furthermore, compared with bulk SrSnO$_3$ and SnO$_2$ nanoparticles, perovskite-

based $SrSnO_3$ NWs displayed the most affinity for the adsorption of OH^- as a substitute of $CO_2^{\bullet-}$, confirming that $SrSnO_3$ NWs show amplified stabilization for $CO_2^{\bullet-}$, which leads to faster kinetics toward formate production.

Various nanostructures based on transition-metal nitrides have been examined for electroreduction reactions; however, a very limited number of these materials have been verified for CO_2 reduction reactions. For instance, Ni_3N was employed for the CO_2 reduction to CO [59]. Yin et al. prepared perovskites based on copper (I) nitride (Cu_3N) nanocubes as a new catalyst for the selective CO_2 reduction to ethylene (C_2H_4) under ambient conditions [60]. These samples were synthesized by the nitridation of copper (II) hydroxide nanowires and were converted into multigrain nanowires to prove their great CO_2 reduction selectivity toward C_2 products, possibly due to the semiconductor properties of Cu_3N. These samples, with perovskite-related ReO_3 structures, can convert CO_2 into ethylene with a faradaic efficiency of about 60% and a Cu mass activity of around 34 A/g in a 0.1 M $KHCO_3$ electrolyte solution at −1.6 V compared with a reversible hydrogen electrode (RHE). Notably, in the products of the gas phase with a molar ratio of >2000 for C_2H_4/CH_4, the Cu_3N catalyst suspends CH_4 formation, and the highest selectivity is realized for CO_2RR by Cu-based catalysis. Through constant electrolysis for 20 h, Cu_3N catalysts are also stable, displaying only a ±7% reduction in FE (from 60 to 53%). In Figure 1a, due to proton reduction in the HER reaction, the current improved after −0.5 V. Under a CO_2 atmosphere, the CV curve is like that under Ar, except that, due to the competition between the CO_2 reduction reaction and the HER, a decrease in the current after −0.5 V is observed. Figure 1b shows the faradaic efficiency related to the potential of ethylene formed with various Cu_3N electrocatalysts. At −0.8 V, the Cu_3N catalyst (25 nm) produces C_2H_4 with an FE = 14%. According to Figure 1c, the maximum FE reaches 60% with a current density of 30 mA/cm^2 and a mass activity of 34 A/g at −1.6 V. Along with C_2H_4, the other samples attained via different potentials contain H_2 with <40% FE (HER) and CO with <9% FE. Other products contain formate and ethanol (<33% FE and <5.7% FE, respectively) over the considered potential range. Figure 1d illustrates the durability of the Cu_3N-catalyzed CO_2-reduction reaction at −1.6 V. After 20 h of sustained electrolysis, the reduction current reduced from 135 mA in the first hour to 101 mA. To investigate the pathway of ethylene formation, that research group used DFT calculations. Their studies showed that the creation of $COCHO_{ads}$ was a main pathway for the conversion of CO_2 to C_2H_4 on the Cu_3N nanocubes because the (100) Cu(I) sites were actively desired for CO−CHO binding (not CO−CO coupling).

Hu et al. have developed new perovskite-type Ti cathodes for CO_2 electrochemical reduction in which there are no alkaline metals: $La_{0.66}Ti_{1-x}Fe_xO_{3\delta}$ (x = 0.2, 0.3, and 0.4, designated as LTF2, LTF3, and LTF4, respectively) [61]. Figure 2 displays the perovskite structure of these cathodes. Compared with Co(II) and Ni(II), Fe(III) cations show outstanding importance in the formation of these compounds. These perovskites exhibit great stability and high catalytic activity for CO_2 reduction. Compared with other reported perovskite cathodes, it is clear that they have less polarization resistance. In a test at 1.2 V and 850 °C for over 300 h, no important degradation of LTF2 was detected, a current density of 0.5 A/cm^2 was shown, and the faradaic efficiency was close to 100%, representing it as a promising feedstock for the CO_2 electrocatalysis to CO. The kinetic procedures study disclosed that the rate-determining step was the electron transfer from the cathode to CO_2.

Chen et al. reported an optimized La_2CuO_4 perovskite catalyst for the electrochemical CO_2RR to methane [62]. La_2CuO_4 is made up of layers of CuO_2 and LaO. Actually, six O atoms surround the Cu atom and the CuO_6 octahedral coordination constructs, leading to an apex-angle-connected octahedron perovskite CuO_2 layer and two layers of LaO that are distinct from the CuO_2 layer. It is predicted that the exceptional electronic structure of La_2CuO_4 would deliver plentiful active sites for the reduction of CO_2. At −1.4 V (vs. RHE), the FE and current density for methane formation reach 56.3% and 117 mA cm^{-2} in the flow-cell configuration, respectively. During the CO_2 reduction process, the structural development of the La_2CuO_4 perovskite occurs simultaneously. As seen in Figure 3a,

compared with the H-cell results, a considerably higher current density (205 mA cm^{-2}) was attained at -1.4 V vs. RHE in 1.0 M KOH purged with CO_2. In addition, the electrolysis steps exhibited improved current density at each potential (Figure 3b). Compared with other products, the CH_4 FE rises with an improved potential. This perovskite catalyst shows a small faradaic efficiency for H_2 (<20%) (Figure 3c). Moreover, a constant and steady CO_2 reduction over CH_4 production was observed via the chronoamperometry test for 1000 s (Figure 3d).
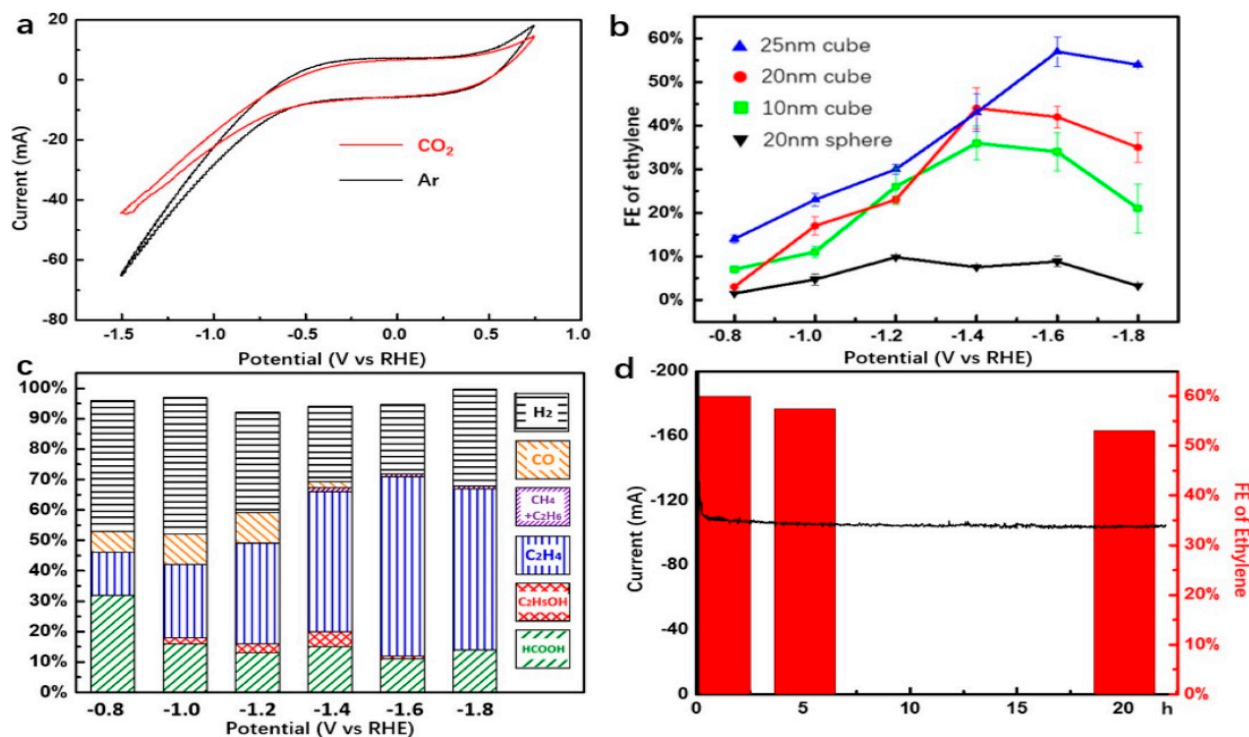
Figure 1. CO_2-reduction reaction with Cu_3N nanocubes in a 0.1 M $KHCO_3$ solution. (**a**) CV curves of the Cu_3N catalyst under Ar (black) and CO_2 (red) atmospheres. (**b**) The FE of ethylene formation by CO_2 reduction in various potentials catalyzed by different Cu_3N nanocubes. (**c**) The different products obtained from the CO_2 reduction produced by Cu_3N (25 nm) at various potentials. (**d**) Ethylene formation faradaic efficiency (red) and the reduction current change (black) during the constant CO_2 reduction catalyzed by NCs (25 nm) at -1.6 V. Adapted with permission from ref. [60]. Copyright 2019 American Chemical Society.
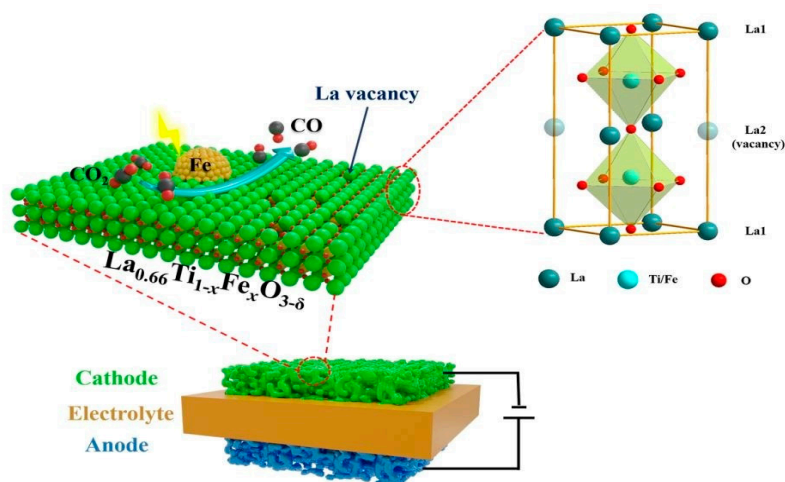
Figure 2. New perovskite-type Ti cathodes with the electrochemical exsolution of Fe nanoparticles. Adapted with permission from ref. [61]. Copyright 2020 Royal Society of Chemistry.
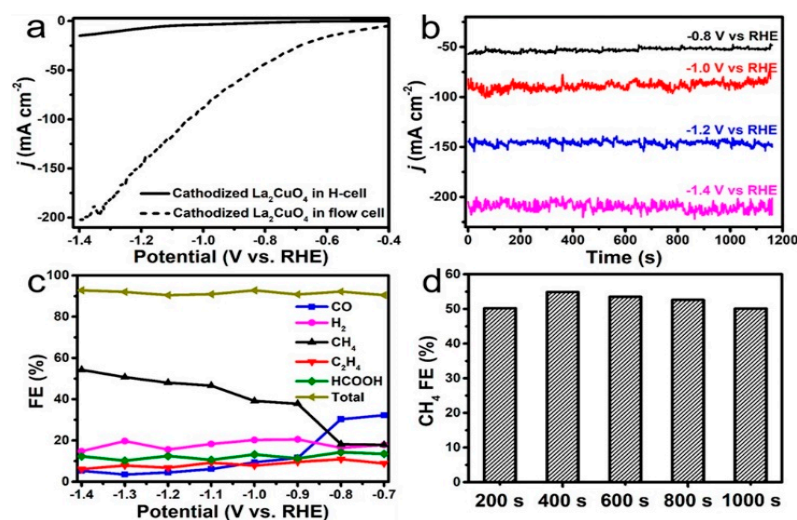
Figure 3. (**a**) LSV (H-cell and flow cell) of the La_2CuO_4 perovskite at a scan rate of 10 mV s^{-1}. (**b**) Potential-dependent steps of electrolysis. (**c**) Faradaic efficiency for samples at different potentials, and (**d**) Faradaic efficiency of CH_4 recorded at -1.4 V versus RHE in the flow cell. Adapted with permission from ref. [62]. Copyright 2020 American Chemical Society.

According to theoretical studies, it can be expected that the Cu atoms relatively reduced to metallic Cu on the surface of the perovskite and the fabricated Cu/La_2CuO_4 are responsible for the superb CO_2 methanization activity. Actually, a greater adsorption of H_xCO (x = 1–3) as an intermediate for the CO_2 methanation is provided by Cu/La_2CuO_4. This study offers an operative new electrocatalyst for the methanation of CO_2 under ambient conditions. Moreover, this study reveals a fundamental understanding of the surface reconstruction during the CO_2 reduction reaction.

Hu et al. developed a perovskite structure of $Sr_2Fe_{1.5-x}Ni_xMo_{0.5}O_{6-\delta}$ (SFNM) (x = 0, 0.05, 0.1, 0.2) denoted as SFM, SFNM-05, SFNM-10, and SFNM-20 respectively, for use as a cathode for the CO_2RR at 800 °C [63]. Solid-oxide electrolysis cells were fabricated for electrochemical analysis, with $Sr_2Fe_{1.5-x}Ni_xMo_{0.5}O$ as the cathode electrode, a mixture of $(La_{0.6}Sr_{0.4})_{0.98}Co_{0.2}Fe_{0.8}O_{3-\delta}$ (LSCF), $Gd_{0.2}Ce_{0.8}O_{2-\delta}$ (GDC), α- ethyl cellulose, and terpineol as the anode paste, and $La_{0.8}Sr_{0.2}Ga_{0.8}Mg_{0.2}O_{3-\delta}$ (LSGM) as the electrolyte. Although Ni plays an imperative role in CO_2 reduction, an increasing Ni-doped catalyst leads to a decrease in reduction performance.

Exploring mechanistically the phase progress of the catalyst would help to develop the activity of CO_2 electroreduction (Figure 4). B-site Fe and Ni cations undergo a reduced reaction under CO as one of the products, and the applied potential creates a reducing environment. Under electroreduction conditions, Ni-doping leads to a reduction in the perovskite durability. In addition, $SrCO_3$ could be grown on the perovskite surface as a result of the reduction of the B-site Fe and Ni elements. Although the existence of the nickel and iron nanoparticles improve the CO_2RR, diffusion of oxidizing species can take place as a result of the additional $SrCO_3$ and carbon deposits, leading to hampered charge transfer on the catalyst surface. Outstandingly, a high FE (99.9%) with a maximum CO yield of 5.26 mlcm^{-2}min^{-1} was obtained under the applied conditions. A 1.5 V, the current densities of the designed samples (SFM, SFNM-05, SFNM-10, and SFNM-20) were 0.95, 0.73, 0.67, and 0.58 A cm^{-2}, respectively. Additionally, the investigation of the effect of different applied voltages on the current densities was documented as a function of time. At lower voltages (1.0 and 1.2 V), the current densities showed little change and the current densities for all samples remained steady throughout the measurement period.
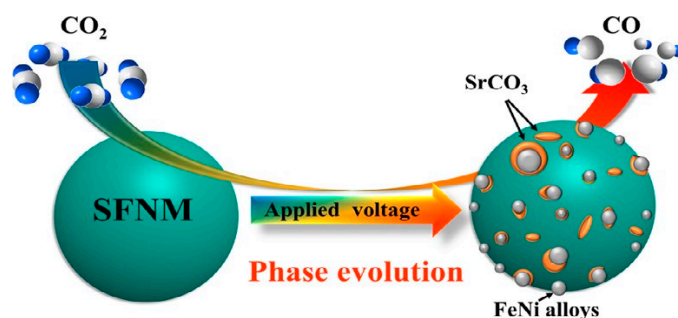
Figure 4. A suggested phase-mechanistic development of an SFNM catalyst for CO_2RR. Adapted with permission from ref. [63]. Copyright 2019 Elsevier.

Ma's research group prepared a type of perovskite oxide (($PrBa)_{0.95}Fe_{1.6}Ni_{0.2}Nb_{0.2}O_{5+\delta}$ (PBFNN)) with $FeNi_3$ nanoalloy deposition on its surface via a reduction procedure for electrochemical CO_2 reduction in solid-oxide electrolysis cells [64]. The as-synthesized perovskite was effectively produced by a sol–gel technique. Following a reduction procedure in H_2/Ar atmosphere (10%) at 800 °C/5h, $FeNi_3$-PBFNN was obtained. Compared with the PBFNN cathode, $FeNi_3$-PBFNN showed more electrocatalytic activity for CO_2RR and led to the production of CO with a FE of 99.3%. This perovskite disclosed a high electrocatalytic activity for CO_2RR because of the plentiful vacancies obtained by the oxygen atoms. The designed perovskite as a cathode displays outstanding stability for 200 h. Moreover, after the stability analysis, the provided SEM images showed that the perovskite cathode reserved the porous structure, and there were no agglomerations between the nanoparticles, which led to the great durability of the CO_2 reduction.

Two bismuth-based halide perovskite composites, $Cs_3Bi_2Br_9/C$ and $Cs_2AgBiBr_6/C$, were prepared for electrochemical CO_2 reduction to HCOOH by Wang et al. [65]. They carried out the electrochemical analyses in acidic media (pH = 2.5) and could directly convert intermediates to formic acid instead of formate. In acidic electrolysis, the two $Cs_3Bi_2Br_9/C$ and $Cs_2AgBiBr_6/C$ composites can successfully inhibit structural degradation. A great FE of 92% at -0.95 V vs. RHE with a current density (j_{HCOOH}) of 133.7 mAcm^{-2} was obtained by $Cs_3Bi_2Br_9/C$, while the $Cs_2AgBiBr_6/C$ show a lower FE (68%) at -1.15 V vs. RHE. More investigation and analyses confirm that the existence of more Bi atoms in $Cs_3Bi_2Br_9$ is a crucial factor to more favorably generate OCHO* intermediates than $Cs_2AgBiBr_6/C$, accelerating the fabrication of HCOOH. Moreover, at -0.95 V over 20 h of electrolysis, for $Cs_3Bi_2Br_9/C$, the current density and FE (~92%) showed no evident decline, while the FE of HCOOH in $Cs_2AgBiBr_6/C$ clearly deteriorated from 68% to 50% at -1.15 V after 10 h. The difference in stability between the two composites could be due to the faster charge transfer and faster increase in the CO_2 conversion ratio for $Cs_3Bi_2Br_9$ than $Cs_2AgBiBr_6$, leading to a reduction in the degradation effect and an enhancement in durability in an aqueous electrolyte.

A nanosized $LaInO_3$ perovskite electrocatalyst was effectively prepared by a simple hydrothermal–calcination method and applied in the electrocatalytic reduction of CO_2 to formate by Zhu et al. [66]. This synthesized electrocatalyst displayed superb activity and excellent selectivity in the CO_2RR. In an aqueous electrolyte solution, CO_2 has low solubility, so its reduction reaction is rigorously restricted in the H-cell, and the current density was very low. So, the flow cell was applied to carry out the CO_2RR. Thus, to solve the problem of solubility and the inadequate mass transfer of CO_2 in an aqueous solution, a suitable setup was designed by the CO_2 diffusion and electrolyte flow-channel-flanked gas-diffusion electrode. The results showed that the current density and faradaic efficiency of $LaInO_3$ in the flow cell was higher than in the H-cell. Electrochemical tests showed that the FE of formate reached up 91.4% (-1.1 V vs. RHE) and the current density of formate was 116.8 mA cm^{-2} (-1.1 V vs. RHE). The results revealed that after 10 h in the flow cell, the FE of formate did not show a considerable reduction, demonstrating that the nanosized $LaInO_3$ perovskite had great stability. Further investigation and DFT calculations exposed

that the activity of the $LaInO_3$ electrocatalyst was due to its intensive adsorption of $CO_2^{\bullet-}$ intermediates.

Bae et al. reported a novel double perovskite, $Pr_{4/3}Ba_{2/3}Co_{2/3}Fe_{2/3}Mn_{2/3}O_{5+\delta}$ (PBCFM), for the CO_2RR in solid-oxide electrochemical cells [67]. Results from different analyses, such as Raman and XRD, proved that the doping of Fe and Mn on the B-site of the perovskite enhanced the CO_2-tolerance of perovskite. Then, they constructed the solid-oxide electrochemical cells with a (Sr, Mg)-doped $LaGaO_3$ (LSGM) electrolyte and the PBCFM-Gd-doped ceria (GDC) electrode. At 1.5 V, the designed electrode revealed a considerably higher current density of 3.76 A cm^{-2} and overapplied potential (1.2 V) at 750 °C for 100 h, and no coking was observed on the electrode surface. The average Faraday efficiency of ~90% obtained by the PBCFM perovskite shows that CO was effectively created from the CO_2RR.

4.2. Photoelectrochemical CO_2 Reduction

Making advances in electrocatalysts and photoelectrocatalytic systems for the selective and efficient production of a target product is a substantial challenge [68–70]. Indeed, perovskite structures with interesting photoconversion and redox properties are always interesting for photoelectrochemical concepts. An $In_{0.4}Bi_{0.6}$ alloy-coated $CH_3NH_3PbI_3$-based photocathode has been demonstrated to produce selective CO_2 reduction with nearly 100% faradaic efficiency (FE) for formic acid production in aqueous solution by Chen et al. [71]. Their examinations revealed that $In_{0.4}Bi_{0.6}$ and $In_{0.6}Bi_{0.2}Sn_{0.2}$ alloys led to more electrocatalytic activity for the selective production of HCOOH as a result of the presence of the In_5Bi_3 phases. The HCOO*, as the intermediate in this procedure, was better stabilized on the In_5Bi_3 phases than on other alloys. At an applied voltage of -1.2 to -1.3 V versus RHE, the highest FE (95−98%) for the production of HCOOH was achieved by the $In_{0.6}Bi_{0.2}Sn_{0.2}$ and $In_{0.4}Bi_{0.6}$ alloys. Next, a favorable method that included coating the perovskite halide with an $In_{0.4}Bi_{0.6}$ alloy was used. With the $In_{0.4}Bi_{0.6}/CH_3NH_3PbI_3$ photocathode, at a low applied potential of -0.52 V vs. RHE under AM 1.5G irradiation, almost 100% FE for formic acid formation could be attained, signifying a 680 mV positive shift relative to the potential detected for the $In_{0.4}Bi_{0.6}$ electrode. At -0.6 V vs. RHE, the faradaic efficiency remained at nearly 100% for at least 1.5 h, and a photo-assisted electrocatalysis efficiency of 7.2% was determined. This photoelectrocatalyst showed a high selectivity for CO_2 reduction to HCOOH.

An organic–inorganic lead–halide perovskite quantum dot of $CH_3NH_3PbBr_3$ and graphene oxide (GO)-wrapped perovskite (GO/$CH_3NH_3PbBr_3$ hybrid) has been reported for the photoelectrochemical conversion of CO_2 into CO and CH_4 as gaseous solar fuels in nonaqueous solutions [72]. A ligand-assisted reprecipitation method was employed for the synthesis of the GO/CH_3NH_3PbBr hybrid via dissolving PbBr2 and CH3NH3Br into the GO/DMF solution assisted by oleylamine and oleic acid (Figure 5a).

LSV analysis was applied to examine the samples for their PEC performances in a cell containing propylene carbonate solution saturated with CO_2 in 0.1 M tetrabutyl ammonium hexafluorophosphate ($TBAPF_6$) (Figure 5b). Compared with the $CH_3NH_3PbBr_3$ quantum dots, GO/$CH_3NH_3PbBr_3$ showed an increase in photocurrents for the photoelectrochemical CO_2 reduction, as the maximum variation of photocurrent was observed at ca. -0.6 V. The photocurrent response of the as-synthesized samples was investigated at -0.6 V (Figure 5c). This voltage was selected from the LSV results. An increase in the photocurrent response was observed for GO/$CH_3NH_3PbBr_3$, while $CH_3NH_3PbBr_3$ showed a decaying photocurrent, suggesting that graphene oxide acts as a stabilizer to preserve $CH_3NH_3PbBr_3$ QDs. Graphene oxide can protect $CH_3NH_3PbBr_3$ quantum dots against degradation by organic solvents and can also act as a charge-transfer intermediate to efficiently distinguish generated electrons and holes. The as-prepared catalyst exhibits an outstanding yield for CO_2 conversion to CO (1.05 µmol cm^{-2} h^{-1}). The chronoamperometric analysis was applied to examine the effect of GO on the stability of $CH_3NH_3PbBr_3$. The photocurrent of $CH_3NH_3PbBr_3$ remained stable for about 1800 s. After introducing GO, the photocathode

produced a long photocurrent for about 6000 s because of the protective effect of GO. As shown in Figure 6, a probable mechanism is suggested for the electrocatalyst to explain the photoreduction of CO_2. The solar-simulated light excited the GO and led to the formation of photoelectrons, using the external-bias-voltage photoelectron transfer to the conduction band of the GO. When a small amount of GO is added onto the perovskite hybrid, a small improvement in photo absorption is observed followed by an improvement in the photocurrent, owing to the role of GO as an intermediate for electron transfer to discrete photogenerated electron–hole pairs. CO_2 is adsorbed onto the surface of GO efficiently and converted to CO and trace amounts of CH_4 because of stingy protons in the organic solvent.
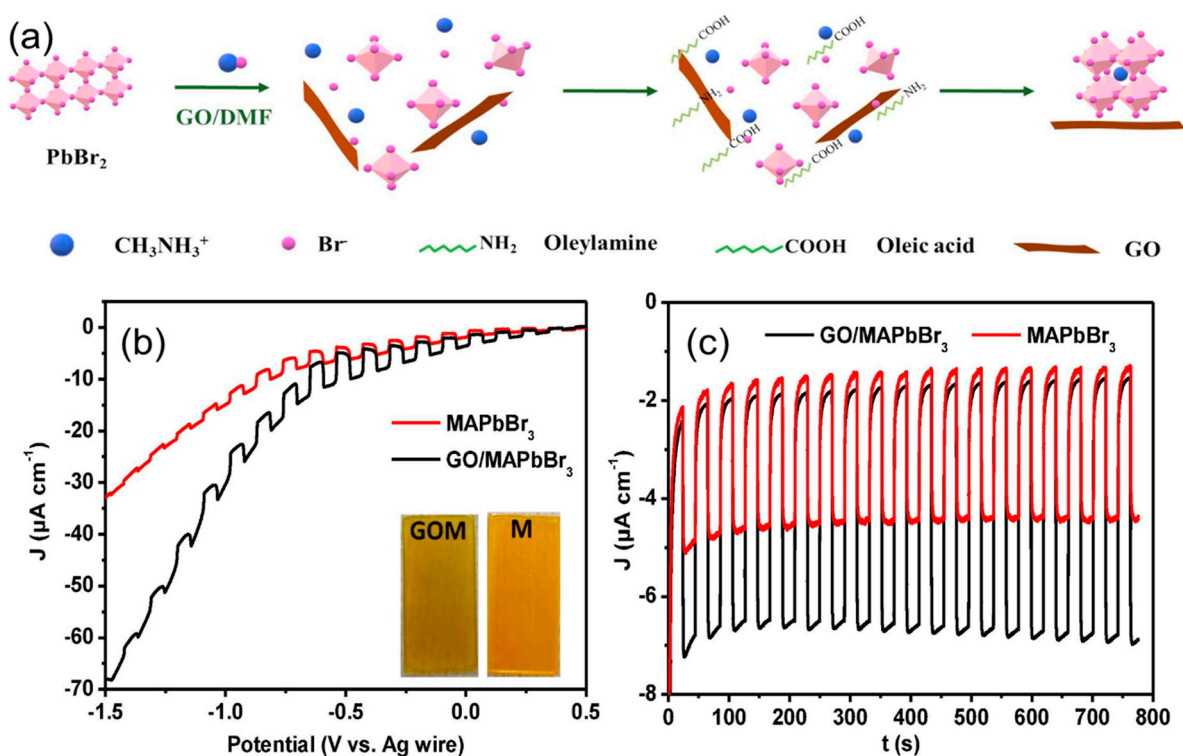
Figure 5. The formation mechanism of the GO/MAPbBr$_3$ hybrid (**a**). LSV of as-obtained samples (**b**). Photocurrent responses of catalysts (in 0.1 M TBAPF$_6$-PC solution) (**c**). Adapted with permission from ref. [72]. Copyright 2019 Elsevier.

Zhang et al. presented a facile construction of a photocathode based on a sandwich-like perovskite with a hydrophobic carbon plate as a capping layer [73]. As shown in Figure 7a, the photocathode contained several layers: first, the hole-transporting layer (NiO), covered on a fluorine-doped tin oxide (FTO) glass; then, the light-absorber perovskite $((Cs_{0.15}FA_{0.85})Pb(I_{0.9}Br_{0.1})_3)$ deposited on the layers. Next, the layer of [6,6]-phenyl-C_{61}-butyric acid methyl ester (PCBM) was deposited on the samples for electron transporting and as a blocking layer of the holes fabricated by ultrathin bathocuproine (BCP). Then, the surface of the blocking layer was coated with a gold layer. On the top of all the layers, a carbon plate was employed to separate the photoactive stack from interaction with water. Furthermore, this carbon plate overcoating acts as a barrier on the perovskite surface and also enables a well-organized transport of the photogenerated electrons for the CO_2 reduction reaction. Once this photocathode was decorated by a cobalt phthalocyanine catalyst (CO_2-saturated 0.5 M KHCO$_3$ and AM1.5G illumination (100 mW cm^{-2})), it displayed an initial potential of 0.58 V with a great photocurrent density of -15.5 mA.cm^{-2}, recorded at -0.11 V (versus RHE), which represents an outstanding performance in this field. Moreover, great durability was obtained for the photoelectrochemical reduction of CO_2 with a constant reaction for 25 h. When IrOx/a-Si as a photoanode was joined to

the photocathode, a photocurrent density of ≈ -3 mA cm^{-2} and a solar-to-CO and total solar-to-fuel energy conversion efficiency of 3.34% and 3.85% were obtained, respectively. These values were much better compared with reported perovskite-based PEC systems. Figure 7b reveals the energy-level diagram of the samples, which shows that CO_2 reduction was effectively performed by the separation and transportation of the photogenerated charge carriers.
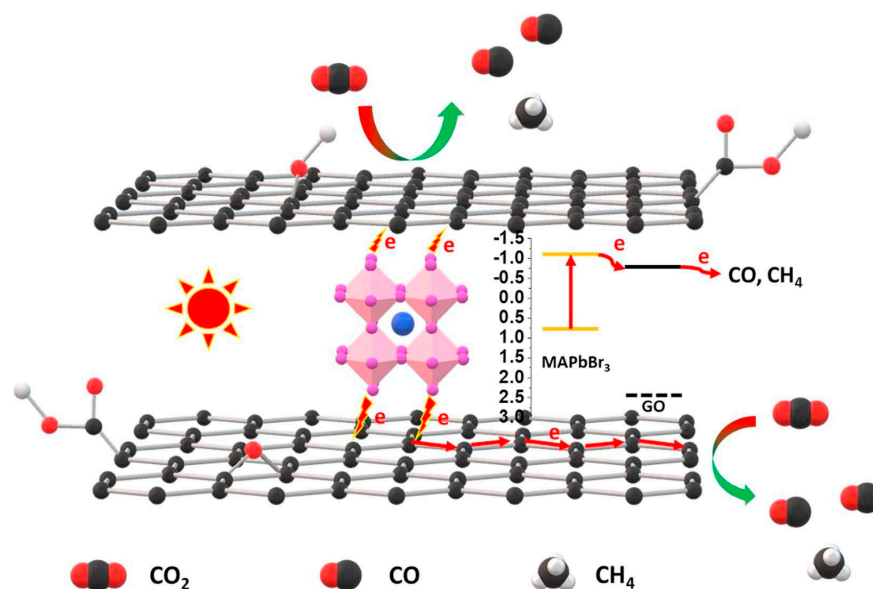
Figure 6. Probable mechanism process of PEC CO_2 reduction. Adapted with permission from ref. [72]. Copyright 2019 Elsevier.
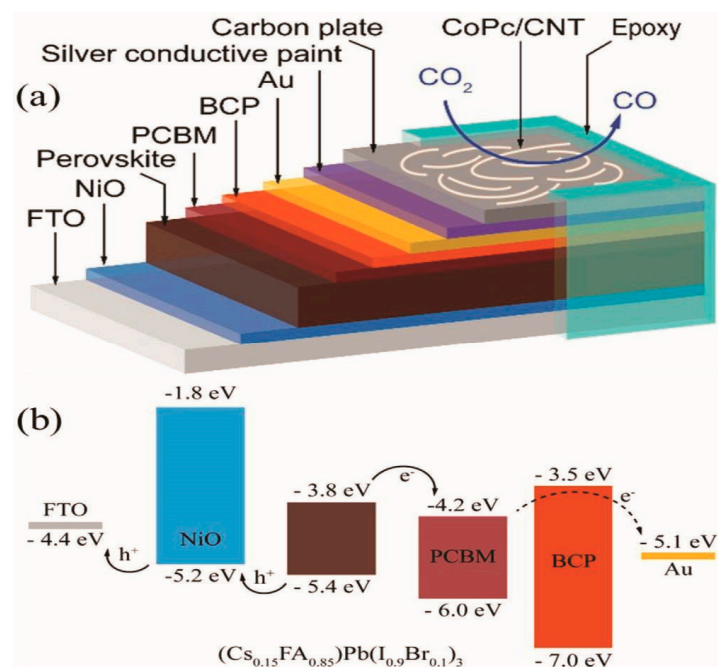
Figure 7. (**a**) Schematic of the carbon-encapsulated perovskite photocathode. (**b**) The energy level diagram of each stack's constituent in the inverted solar-cell structure. Adapted with permission from ref. [73]. Copyright 2020 Wiley.

This study demonstrates that efficient and durable perovskite-based PEC electrodes can be achieved through elaborate interface design and engineering.

A PEC system based on a Au-decorated ZnO@ZnTe@CdTe photocathode and $CH_3NH_3PbI_3$ perovskite tandem cell has been verified by Jang et al. as an unbiased solar-driven CO_2 reduction to CO [74]. The designed cell disclosed a stable efficiency of solar-to-CO of above 0.35% with a faradaic efficiency of over 80% and a solar-to-fuel efficiency of more than 0.43%, with H_2 as a byproduct. This PEC cell showed the selective CO creation from CO_2 reduction using an operative photocathode−perovskite tandem device working in sunlight without an exterior bias. The overpotential was decreased by the ternary photocathode, and the $CH_3NH_3PbI_3$ perovskite generated a voltage that is sufficient to initiate the reduction of CO_2 without an exterior bias. Furthermore, the operative light harvesting to the NIR area of the solar range, which is transferred over the photocathodes, was simplified by the high absorption coefficient of the $CH_3NH_3PbI_3$ perovskite.

Zhang and his colleagues prepared a photocathode based on a $CsPbBr_3$ (CPB) thin-film for photoelectrochemical CO_2 reduction [75]. A three-electrode system was designed for PEC analyses by a Pt foil and Ag/AgCl (3M KCl) as the counter electrode and the reference electrode, respectively. They used a two-step process to obtain thin-layer films. First, they applied a layer of $PbBr_2$ films using a spin-coating process. Then, the solutions containing the CsBr-based materials were applied onto the surface using the spin-coating technique, repeating the process four times. Next, they added fluorine, Nafion, and Au in the CsBr solution to obtain $CsPbBr_3$-F-N-Au thin films. By adding F ions into the $CsPbBr_3$ structure, an enhancement in the chemical interactions and a reduction in the trap density of the $CsPbBr_3$ layers was created. In addition, the band gap of the perovskites was adjusted by the introduction of Nafion, and the trap density was reduced, leading to hindering of the charge carrier transfer, which intensified the charge recombination in the obtained perovskites. Then, by adding Au, separation of the photoinduced charge carriers was facilitated in the photocathode. At a potential of -0.5 V (vs. Ag/AgCl) at a 4.13 mW cm^{-2} light radiance, the designed photocathode revealed the best PEC performance, containing the highest photocurrent of -0.23 mA cm^{-2} which is twice as much as the pristine $CsPbBr_3$ photocathode. This study showed that a halide-perovskite-based photocathode can be directly used to help reduce carbon dioxide.

4.3. Photovoltaic–Electrochemical CO_2 Reduction

Artificial photosynthesis, a technological device that uses solar irradiation as an energy source and water as an electron source to convert carbon dioxide into energy-dense organic compounds (fuels or other carbons for the chemical industry), is attractive in specific contexts [76]. This can be achieved in an integrated cell by using photovoltaic (PV) cells to supply photoelectrons and holes to be used in an electrochemical cell (EC) to oxidize water at the anode and to reduce carbon dioxide at the cathode, creating a PV-EC reference system to reduce CO_2 to fuels. The PV-EC systems can be classified into two general configurations, namely monolithic and polylithic. In a monolithic configuration, the junction terminals of the photovoltaic cell is directly connected to the anode and cathode of the EC unit, and the direct-circuit (DC) photogenerated power is designed to be used in the electrocatalytic process without any external electrical connections and/or inversion, while in a polylithic configuration, the PV and EC cells work separately, and the electrical power of the PV cell can be used in the electrochemical cell usually after a DC/DC inversion. Generally, the polylithic PV-EC has significantly better controllability of product selectivity, e.g., increasing the applied voltage via the series connection of PV modules and easier matching of the operating current by using certain ratios of the PV and EC areas. However, the expected levelized cost of the CO_2 reduction product (LCOC) will be higher in the polylithic configuration in comparison with the monolithic configuration, which has lower complexity and fewer external accessories.

Huan et al. provided a new catalyst for CO_2 conversion to hydrocarbons, which exhibited a faradaic yield of 62% in product generation [77]. This three-layer catalyst contains a metal Cu core protected by layers of CuO and Cu_2O (Figure 8a). Remarkably, over a 60 min electrolysis at -0.95 V versus RHE, the structure of the CuO cathode changed.

When joined with an advanced, low-cost perovskite photovoltaic minimodule, this PV-EC device achieves a solar-to-fuel value of 2.3% by combining it with a mini-module perovskite photovoltaic device recognized using two sequences of three perovskite photovoltaics with an active area of 0.25 cm^2 coupled in parallel (Figure 8b), offering a yardstick for PV-EC systems that includes plentiful earth-abundant elements. To examine the CO_2-reduction performance on this system, current–voltage measurements of the modules were applied, which exposed a high photo-to-current efficiency (17.5%) at 2.45 V and 10.0 mA. A constant current of 6.0 ± 0.2 mA with a current density of ~18 mA·cm^{-2} and a potential of 2.8 ± 0.02 (V) were proved by the connection of both systems. Over a 50 min electrolysis by using the gas chromatography (GC) technique and analyzing the reduction products, it was shown that the PV-EC catalyst generates a steady current.
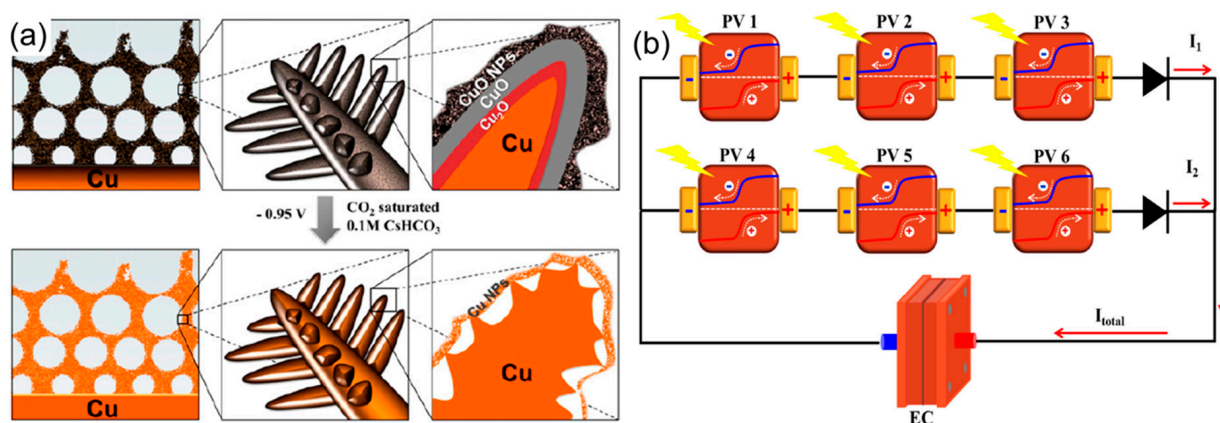
Figure 8. (**a**) Schematic of the CuO sample before (top) and after (bottom) CO_2 electroreduction in a 0.1 M $CsHCO_3$ electrolyte. (**b**) Schematic illustration of the perovskite mini-module that was recognized via the joining of six PV cells attached to the electrolyzer. Adapted with permission from ref. [77]. Copyright 2019 PNAS.

By using water as an electron source, Schreier et al. demonstrated a well-organized conversion of solar-driven CO_2 to CO with a 90% faradaic efficiency [78]. Figure 9a shows the designed setup fabricated by an electrochemical cell with oxidized gold as the cathode, IrO_2 as the anode in a 0.5 M $NaHCO_3$ electrolyte connected to perovskite photovoltaics. For monitoring of the produced samples, the gas chromatography technique was employed in situ. Figure 9b displays the energy diagram for the CO_2 conversion to CO with three series-connected perovskite solar cells, which created enough voltage to overcome the free energy of the reaction (ΔE) and the reaction overpotential (η) at the cells. A solar-to-fuel efficiency of 6.5% and 7% was obtained for CO as the main product and hydrogen as a by-product, respectively. Also, this study evidenced a prolonged, steady operation of photovoltaics based on perovskite with high open-circuit voltage. For more than 18 h, the current density was constant at approximately 5.8 mA cm^{-2}, and the slight change in the photocurrent was detected.

In another work, Esiner and colleagues revealed p-i-n lead–halide perovskite solar cells combined with RuO_2 as an anode and Au as a cathode for the CO_2 reduction to CO and CH_4 via water oxidation in neutral pH media [79]. This prepared system showed a solar-to-CO efficiency of >8% with faradaic efficiencies upward of 80%. Comprising hydrogen creation, the total efficiency of the solar-to-fuel step remains at >8.3% for 10 h. Additionally, using a system based on a four-series-coupled perovskite with copper and RuO_2 electrodes, methane was formed as the main product with a conversion efficiency of 2% and H_2 with a 3% conversion efficiency, and the solar-driven fuel conversion efficiency was 5% for an 8 h procedure with the PV-EC device.
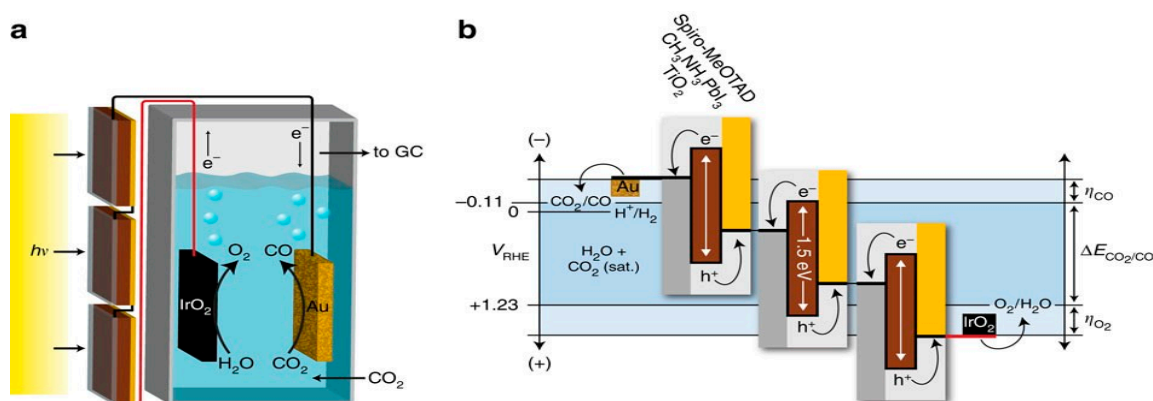
Figure 9. (**a**) Schematic of the PV-EC unit. (**b**) Energy diagram for CO_2 reduction to CO with three perovskite solar cells. Adapted with permission from ref. [78]. Copyright 2015 Springer Nature.

Zhang and colleagues reported a new electrocatalyst for CO_2RR using some metals attached onto Zr6-cluster-porphyrin-framework hollow nanocapsules (M-SAs/Zr-CPF) connected to a custom-built large-area $[Cs_{0.05}(FA_{0.85}MA_{0.15})_{0.95}]Pb_{0.9}(I_{0.85}Br_{0.15})_3$ perovskite solar cell [80]. These designed electrocatalysts with hollow structures simplify electron transfer and CO_2 adsorption. Among the different metals, the Co atom showed improved electrocatalytic activity in the energy reduction of *COOH formation and *CO desorption. Coupled with a RuO_2/C anode in a 0.1 M $KHCO_3$ aqueous solution within an H-type electrolytic cell separated by a Nafion-117 membrane, the electrocatalyst showed a substantial faradaic efficiency, low overpotential, and great stability for CO_2 reduction with a solar-to-CO energy conversion efficiency of 12.5%. Under AM 1.5G illumination, the electrocatalyst showed a total power conversion efficiency (PCE) of 21.3% with an open-circuit voltage (V_{oc}) of 4.6 V and a short-circuit current density (J_{sc}) of 8.96 mA cm^{-2}, and the optimal working voltage and current was 3.2 V and 3.2 mA, respectively. The long-term stability tests of M-SAs/Zr-CPF CO2RR-OER showed a steady working voltage of 3.1 V, and the current density was retained at ~3.2 mA cm^{-2}, with an FE_{CO} of 58.5% over the 3 h of electrolysis. In Table 2, we reviewed the recent progress in perovskites for their roles in EC, PEC, and PV-EC CO_2 reduction.

Table 2. Perovskites for EC, PEC, and PV-EC CO_2 reduction.

Cathode/Photocathode	Anode/Photoanode	PV Absorber	Method	CO_2RR Product	FE%	Solar-to-Product Efficiency	References
$Sr_2Fe_{1.5}Mo_{0.5}O_{6-\delta}$	Pt plate	-	EC	CO	95	-	[57]
$SrSnO_3$ nanowires	Pt wire	-	EC	HCO_2^-	80	-	[58]
Cu_3N nanocubes	-	-	EC	C_2H_4	60	-	[60]
$La_{0.66}Ti_{1-x}Fe_xO_{3\delta}$	$Gd_{0.2}Ce_{0.8}O_{2-\delta}$	-	EC	CO	~100	-	[61]
La_2CuO_4	-	-	EC	CH_4	56.3	-	[62]
$Sr_2\,Fe_{1.5-x}\,Ni_xMo_{0.5}O_{6-\delta}$	$(La_{0.6}Sr_{0.4})_{0.98}$ $Co_{0.2}Fe_{0.8}O_{3-\delta}$, $Gd_{0.2}Ce_{0.8}O_{2-\delta}$	-	EC	CO	99.9	-	[63]
$(PrBa)_{0.95}Fe_{1.6}Ni_{0.2}Nb_{0.2}O_{5+\delta}$	$La_{0.6}Sr_{0.4}\,Co_{0.2}Fe_{0.8}O_{3-\delta}$	-	EC	CO	99.3	-	[64]
$Cs_3Bi_2Br_9/C$	Pt foil	-	EC	HCOOH	92	-	[65]
$LaInO_3$	Ni foam	-	EC	$HCOO^-$	91.4	-	[66]
$Pr_{4/3}Ba_{2/3}Co_{2/3}Fe_{2/3}Mn_{2/3}O_{5+\delta}/$ Gd-doped ceria	-	-	EC	CO	90	-	[67]
$In_{0.4}Bi_{0.6}$ alloy-coated $CH_3NH_3PbI_3$	Pt	-	PEC	HCOOH	~100	7.2	[71]
$GO/CH_3NH_3PbBr_3$	Pt wire	-	PEC	CO and CH_4	-	-	[72]
$(Cs_{0.15}FA_{0.85})Pb(I_{0.9}Br_{0.1})_3$	Si photoanode	-	PEC	CO	88	3.85	[73]
ZnO@ZnTe@CdTe $/CH_3NH_3PbI_3$ perovskite tandem cell	Cobalt–bicarbonate	-	PEC	CO	~80%	0.43%	[74]
$CsPbBr_3$-F-N-Au	Pt foil	-	PEC	CO	-	-	[75]
Dendritic-nanostructured CuO	Dendritic-nanostructured CuO	GaInP/GaInAs/Ge	PV-EC	hydrocarbons	62	2.3	[77]
Oxidized Au	IrO_2	$CH_3NH_3PbI_3$	PV-EC	CO	90	6.5	[78]
Au wire	RuO2	$(HC(NH_2)_2)_{0.66}(CH_3NH_3)_{0.34}PbI_{2.85}Br_{0.15}$	PV-EC	CO	80	>8%	[79]
Co-SAs/Zr-CPF	RuO_2/C	$Cs_{0.05}(FA_{0.85}MA_{0.15})_{0.95}]Pb_{0.9}(I_{0.85}Br_{0.15})_3$	PV-EC	CO	>50	12.5	[80]

5. Conclusions and Perspectives

The conversion of CO_2 to added-value chemicals or fuels is an attractive strategy for storing such a renewable source of energy into the form of chemical energy. The catalysis technology has received more and more attention for such a concept. Therefore, in parallel to more developed systems for electrochemical water splitting, the utility of innovative and advanced catalysts to develop critical performance factors, e.g., durability, conversion efficiency, and energy/power densities, must be explored in the specific concept of the CO_2RR. To achieve this purpose, the scientific community has been working on the construction of new materials that allow the design of advanced electrode systems for efficient CO_2 capture and reduction. Recently, perovskite-based catalysts have drawn a growing interest in various sectors from renewable energy to environmental processes. We have reviewed the various kinds of perovskites, followed by a discussion of their recent progress in their application as an emerging functional material in EC, PEC, and PV-EC reactions for CO_2 reduction. Perovskite oxides have shown more potential in EC CO_2RRs because of their oxygen vacancy sites and lattice distortions, which create more active sites for electrochemical CO_2 reduction. Moreover, perovskite oxides have more stability under harsh conditions like high temperature and can be used for solid-oxide fuel cells. Due to the presence of halide ions, halide perovskites show higher absorption coefficients and have more carrier mobilities, which make them more suitable for PEC and PV-EC CO_2 reduction [81,82]. To achieve outstanding perovskite-based electrocatalysts, there are various strategies available, including developing the intrinsic activity and increasing available active sites by defect engineering on the perovskite surface, crystal structure regulation, tuning the electrical conductivity and synthesis process, and surface modification. High electron transfer of perovskites leads to the reduction of ohmic losses and the evolution of active sites, developing electrocatalytic performance. To increase electronic conductivity, some strategies such as using electrically conductive materials and doping agents are beneficial. In addition, cations in A- and B-sites have a critical role in adjusting the electron arrangement, thereby affecting the electrical conductivity and increasing the electrocatalytic activity. However, despite substantial development having been made, there are still a large number of perovskites that are theoretically predicted to exist, and their application as catalysts has also never been investigated experimentally. In fact, the research on the electrocatalytic applications of perovskites for CO_2 reduction is still at its initial stages, and some challenges are still waiting to be addressed to facilitate their practical applications. One of the crucial challenges is the stability of perovskites in the aqueous solution of EC cells, which can be improved by doping, barrier layers, crystal engineering, and encapsulation approaches. Another issue is the toxicity of lead in some kinds of halide perovskites from the aspect of environmental concerns, which can be addressed by replacement with other more eco-friendly components e.g., Ti, Bi, or by using lead-leakage-preventing layers during encapsulation of the system. Also, in terms of industrial and commercial production, the fabrication of perovskite-based electrocatalysts with uniform particle size, identical morphology, and high specific surface area is still a main problem. Developing well-organized and cost-effective manufacturing procedures is crucial for scaling up perovskite-based CO_2RR. This can be achieved through the optimization of reaction conditions and by developing new production technologies. Researchers can explore ways to reduce the cost of raw materials and improve the efficiency of perovskite production. This can include using cheaper precursors, optimizing reaction conditions, and developing new synthesis methods. Also, perovskite-based CO_2RR can be integrated with existing industrial processes to improve efficiency. In addition, to achieve practical objectives, electrocatalysts must be able to work at high current densities for hundreds of hours, while in the laboratory, the analyses can be performed in a short period of time, so it is essential to improve the stability of these compounds [83]. Moreover, more studies on the electroreduction of CO_2 by perovskites are necessary to further promote improvements in this field.

References

1. Zhang, S.; Jing, X.; Wang, Y.; Li, F. Towards Carbon-Neutral Methanol Production from Carbon Dioxide Electroreduction. *ChemNanoMat* **2021**, *7*, 728–736. [CrossRef]
2. Wu, H.; Yuan, Y.; Chen, Y.; Lv, D.; Tu, S.; Wu, Y.; Li, Z.; Xia, Q. Highly Efficient Capture of Postcombustion Generated CO_2 through a Copper-Based Metal-Organic Framework. *Energy Fuels* **2021**, *35*, 610–617. [CrossRef]
3. Zhang, S.; Kang, P.; Meyer, T.J. Nanostructured tin catalysts for selective electrochemical reduction of carbon dioxide to formate. *J. Am. Chem. Soc.* **2014**, *136*, 1734–1737. [CrossRef] [PubMed]
4. Zheng, Y.; Wang, S.; Pan, Z.; Yin, B. Electrochemical CO_2 reduction to CO using solid oxide electrolysis cells with high-performance Ta-doped bismuth strontium ferrite air electrode. *Energy* **2021**, *228*, 120579. [CrossRef]
5. Zhang, S.; Fan, Q.; Xia, R.; Meyer, T.J. CO_2 Reduction: From Homogeneous to Heterogeneous Electrocatalysis. *Acc. Chem. Res.* **2020**, *53*, 255–264. [CrossRef] [PubMed]
6. Li, Y.; Sun, Q. Recent Advances in Breaking Scaling Relations for Effective Electrochemical Conversion of CO_2. *Adv. Energy Mater* **2016**, *6*, 1600463. [CrossRef]
7. Aresta, M.; Dibenedetto, A. Utilisation of CO_2 as a chemical feedstock: Opportunities and challenges. *Dalt. Trans.* **2007**, *28*, 2975–2992. [CrossRef]
8. Whipple, D.T.; Kenis, P.J.A. Prospects of CO_2 utilization via direct heterogeneous electrochemical reduction. *J. Phys. Chem. Lett.* **2010**, *1*, 3451–3458. [CrossRef]
9. Creissen, C.E.; Fontecave, M. Solar-Driven Electrochemical CO_2 Reduction with Heterogeneous Catalysts. *Adv. Energy Mater.* **2021**, *11*, 2002652. [CrossRef]
10. Bin, A.R.; Yusoff, M.; Jang, J. Highly efficient photoelectrochemical water splitting by a hybrid tandem perovskite solar cell. *Chem. Commun.* **2016**, *52*, 5824–5827. [CrossRef]
11. Zhu, D.D.; Liu, J.L.; Qiao, S.Z. Recent Advances in Inorganic Heterogeneous Electrocatalysts for Reduction of Carbon Dioxide. *Adv. Mater.* **2016**, *28*, 3423–3452. [CrossRef] [PubMed]
12. Kumar, B.; Atla, V.; Brian, J.P.; Kumari, S.; Nguyen, T.Q.; Sunkara, M.; Spurgeon, J.M. Reduced SnO_2 Porous Nanowires with a High Density of Grain Boundaries as Catalysts for Efficient Electrochemical CO_2-into-HCOOH Conversion. *Angew. Chem. Int. Ed.* **2017**, *56*, 3645–3649. [CrossRef] [PubMed]
13. Gu, J.; Héroguel, F.; Luterbacher, J.; Hu, X. Densely Packed, Ultra Small SnO Nanoparticles for Enhanced Activity and Selectivity in Electrochemical CO_2 Reduction. *Angew. Chem.* **2018**, *130*, 2993–2997. [CrossRef]
14. Liu, Y.; Chen, S.; Quan, X.; Yu, H. Efficient Electrochemical Reduction of Carbon Dioxide to Acetate on Nitrogen-Doped Nanodiamond. *J. Am. Chem. Soc.* **2015**, *137*, 11631–11636. [CrossRef] [PubMed]
15. Wu, J.; Yadav, R.M.; Liu, M.; Sharma, P.P.; Tiwary, C.S.; Ma, L.; Zou, X.; Zhou, X.D.; Yakobson, B.I.; Lou, J.; et al. Achieving highly efficient, selective, and stable CO_2 reduction on nitrogen-doped carbon nanotubes. *ACS Nano* **2015**, *9*, 5364–5371. [CrossRef] [PubMed]
16. Zendehdel, M.; Yaghoobi Nia, N.; Paci, B.; Generosi, A.; Di Carlo, A. Zero-Waste Scalable Blade-Spin Coating as Universal Approach for Layer-By-Layer Deposition of 3D/2D Perovskite Films in High Efficiency Perovskite Solar Modules. *Sol. RRL* **2021**, *6*, 2100637. [CrossRef]
17. Yaghoobi Nia, N.; Saranin, D.; Palma, A.L.; Di Carlo, A. Perovskite solar cells. In *Solar Cells and Light Management*; Elsevier: Amsterdam, The Netherlands, 2020; pp. 163–228.
18. Zhang, H.T.; Park, T.J.; Islam, A.N.M.N.; Tran, D.S.J.; Manna, S.; Wang, Q.; Mondal, S.; Yu, H.; Banik, S.; Cheng, S.; et al. Reconfigurable perovskite nickelate electronics for artificial intelligence. *Science* **2022**, *375*, 533–539. [CrossRef]
19. Sutherland, B.R.; Sargent, E.H. Perovskite photonic sources. *Nat. Photonics* **2016**, *10*, 295–302. [CrossRef]
20. Tofanello, A.; Freitas, A.L.M.; de Queiroz, T.B.; Bonadio, A.; Martinho, H.; Souza, J.A. Magnetism in a 2D Hybrid Ruddlesden–Popper Perovskite through Charge Redistribution Driven by an Organic Functional Spacer. *J. Phys. Chem. Lett.* **2022**, *13*, 1406–1415. [CrossRef]

21. Hwang, J.; Rao, R.R.; Giordano, L.; Katayama, Y.; Yu, Y.; Shao-Horn, Y. Perovskites in catalysis and electrocatalysis. *Science* **2017**, *358*, 751–756. [CrossRef]

22. Zendehdel, M.; Yaghoobi Nia, N.; Yaghoubinia, M. Emerging Thin Film Solar Panels. In *Reliability and Ecological Aspects of Photovoltaic Modules*; IntechOpen: London, UK, 2020.

23. Sun, H.; Dai, J.; Zhou, W.; Shao, Z. Emerging Strategies for Developing High-Performance Perovskite-Based Materials for Electrochemical Water Splitting. *Energy Fuels* **2020**, *34*, 10547–10567. [CrossRef]

24. Liang, J.; Chen, D.; Yao, X.; Zhang, K.; Qu, F.; Qin, L.; Huang, Y.; Li, J. Recent Progress and Development in Inorganic Halide Perovskite Quantum Dots for Photoelectrochemical Applications. *Small* **2020**, *16*, 1903398. [CrossRef] [PubMed]

25. Zhao, B.; Yan, B.; Jiang, Z.; Yao, S.; Liu, Z.; Wu, Q.; Ran, R.; Senanayake, S.D.; Weng, D.; Chen, J.G. High selectivity of CO_2 hydrogenation to CO by controlling the valence state of nickel using perovskite. *Chem. Commun.* **2018**, *54*, 7354–7357. [CrossRef]

26. Goel, P.; Sundriyal, S.; Shrivastav, V.; Mishra, S.; Dubal, D.P.; Kim, K.H.; Deep, A. Perovskite materials as superior and powerful platforms for energy conversion and storage applications. *Nano Energy* **2021**, *80*, 105552. [CrossRef]

27. Yin, W.J.; Weng, B.; Ge, J.; Sun, Q.; Li, Z.; Yan, Y. Oxide perovskites, double perovskites and derivatives for electrocatalysis, photocatalysis, and photovoltaics. *Energy Environ. Sci.* **2019**, *12*, 442–462. [CrossRef]

28. Li, X.; Zhao, H.; Liang, J.; Luo, Y.; Chen, G.; Shi, X.; Lu, S.; Gao, S.; Hu, J.; Liu, Q.; et al. A-site perovskite oxides: An emerging functional material for electrocatalysis and photocatalysis. *J. Mater. Chem. A* **2021**, *9*, 6650–6670. [CrossRef]

29. Porta, P.; De Rossi, S.; Faticanti, M.; Minelli, G.; Pettiti, I.; Lisi, L.; Turco, M. Perovskite-Type Oxides: I. Structural, Magnetic, and Morphological Properties of $LaMn_{1-x}Cu_xO_3$ and $LaCo_{1-x}Cu_xO_3$ Solid Solutions with Large Surface Area. *J. Solid State Chem.* **1999**, *146*, 291–304. [CrossRef]

30. Wei, W.J.; Li, C.; Li, L.S.; Tang, Y.Z.; Jiang, X.X.; Lin, Z.S. Phase transition, optical and dielectric properties regulated by anion-substitution in a homologous series of 2D hybrid organic–inorganic perovskites. *J. Mater. Chem. C* **2019**, *7*, 11964–11971. [CrossRef]

31. Song, K.W.; Lee, K.T. Characterization of Ba0.5Sr0.5M1−xFexO3−δ (M = Co and Cu) perovskite oxide cathode materials for intermediate temperature solid oxide fuel cells. *Ceram. Int.* **2012**, *38*, 5123–5131. [CrossRef]

32. Devi, S.; Taxak, V.B.; Chahar, S.; Dalal, M.; Dalal, J.; Hooda, A.; Khatkar, A.; Malik, R.K.; Khatkar, S.P. Crystal chemistry and optical analysis of a novel perovskite type SrLa2Al2O7:Sm3+ nanophosphor for white LEDs. *Ceram. Int.* **2019**, *45*, 15571–15579. [CrossRef]

33. Zhang, L.; Hu, J.; Song, P.; Qin, H.; Jiang, M. Electrical properties and ethanol-sensing characteristics of perovskite La1 − xPbxFeO3. *Sens. Actuators B Chem.* **2006**, *114*, 836–840. [CrossRef]

34. Bhat, A.A.; Khandy, S.A.; Islam, I.; Tomar, R. Optical, electrochemical and photocatalytic properties of cobalt doped CsPbCl3 nanostructures: A one-pot synthesis approach. *Sci. Rep.* **2021**, *11*, 16473. [CrossRef]

35. Islam, I.; Khandy, S.A.; Zaman, M.B.; Hafiz, A.K.; Siddiqui, A.M.; Chai, J.-D. Growth and characterization of crystalline BaSnO3 perovskite nanostructures and the influence of heavy Mn doping on its properties. *J. Alloys Compd.* **2021**, *867*, 158900. [CrossRef]

36. Khandy, S.A.; Vaid, S.G.; Islam, I.; Hafiz, A.K.; Chai, J.-D. Understanding the stability concerns and electronic structure of CsYbX3 (X=Cl,Br) halidoperovskites for optoelectronic applications. *J. Alloys Compd.* **2021**, *867*, 158966. [CrossRef]

37. Babu, R.; Giribabu, L.; Singh, S.P. Recent Advances in Halide-Based Perovskite Crystals and Their Optoelectronic Applications. Cryst. *Growth Des.* **2018**, *18*, 2645–2664. [CrossRef]

38. Yaghubinia, M.; Ebnali, M.; Zendehdel, M.; Yaghoubinia, M. Improvement of perovskite solar cells photovoltaic performance by localized surface plasmon effect of silver-alumina core-shell nanoparticles. In Proceedings of the PHOTOPTICS 2016-Proceedings of the 4th International Conference on Photonics, Optics and Laser Technology, Rome, Italy, 27–29 February 2016.

39. Di Carlo, A.; Yaghoobi Nia, N.; Zendehdel, M.; Agresti, A.; Pescetelli, S.; Vesce, L.; Castriotta, L.A.; Matteocci, F.; Di Giacomo, F.; Saranin, D.; et al. Halide perovskite modules and panels. In *Proceedings of the nanoGe Spring Meeting 2022*; Fundació Scito: València, Spain, 2022.

40. Yaghoobi Nia, N.; Zendehdel, M.; Abdi-Jalebi, M.; Castriotta, L.A.; Kosasih, F.U.; Lamanna, E.; Abolhasani, M.M.; Zheng, Z.; Andaji-Garmaroudi, Z.; Asadi, K.; et al. Beyond 17% stable perovskite solar module via polaron arrangement of tuned polymeric hole transport layer. *Nano Energy* **2021**, *82*, 105685. [CrossRef]

41. Schmidt, L.C.; Pertegás, A.; González-Carrero, S.; Malinkiewicz, O.; Agouram, S.; Espallargas, G.M.; Bolink, H.J.; Galian, R.E.; Pérez-Prieto, J. Nontemplate synthesis of CH3NH3PbBr3 perovskite nanoparticles. *J. Am. Chem. Soc.* **2014**, *136*, 850–853. [CrossRef] [PubMed]

42. Yaghoobi Nia, N.; Lamanna, E.; Zendehdel, M.; Palma, A.L.; Zurlo, F.; Castriotta, L.A.; Di Carlo, A. Doping Strategy for Efficient and Stable Triple Cation Hybrid Perovskite Solar Cells and Module Based on Poly(3-hexylthiophene) Hole Transport Layer. *Small* **2019**, *15*, 1904399. [CrossRef]

43. Hao, F.; Stoumpos, C.C.; Cao, D.H.; Chang, R.P.H.; Kanatzidis, M.G. Lead-free solid-state organic–inorganic halide perovskite solar cells. *Nat. Photonics* **2014**, *8*, 489–494. [CrossRef]

44. Sardashti, M.K.; Zendehdel, M.; Yaghoobi Nia, N.; Karimian, D.; Sheikhi, M. High Efficiency MAPbI 3 Perovskite Solar Cell Using a Pure Thin Film of Polyoxometalate as Scaffold Layer. *ChemSusChem* **2017**, *10*, 3773–3779. [CrossRef]

45. Li, Y.F.; Chou, S.Y.; Huang, P.; Xiao, C.; Liu, X.; Xie, Y.; Zhao, F.; Huang, Y.; Feng, J.; Zhong, H.; et al. Stretchable Organometal-Halide-Perovskite Quantum-Dot Light-Emitting Diodes. *Adv. Mater.* **2019**, *31*, 1807516. [CrossRef] [PubMed]

46. Navazani, S.; Yaghoobi Nia, N.; Zendehdel, M.; Shokuhfar, A.; Di Carlo, A. Fabrication of high efficiency, low-temperature planar perovskite solar cells via scalable double-step crystal engineering deposition method fully out of glove box. *Sol. Energy* **2020**, *206*, 181–187. [CrossRef]

47. Ermanova, I.; Yaghoobi Nia, N.; Lamanna, E.; Di Bartolomeo, E.; Kolesnikov, E.; Luchnikov, L.; Di Carlo, A. Crystal Engineering Approach for Fabrication of Inverted Perovskite Solar Cell in Ambient Conditions. *Energies* **2021**, *14*, 1751. [CrossRef]

48. Castriotta, L.A.; Zendehdel, M.; Yaghoobi Nia, N.; Leonardi, E.; Löffler, M.; Paci, B.; Generosi, A.; Rellinghaus, B.; Di Carlo, A. Reducing Losses in Perovskite Large Area Solar Technology: Laser Design Optimization for Highly Efficient Modules and Mini Panels. *Adv. Energy Mater* **2022**, *12*, 2103420. [CrossRef]

49. Zhang, H.; Darabi, K.; Yaghoobi Nia, N.; Krishna, A.; Ahlawat, P.; Guo, B.; Almalki, M.H.S.; Su, T.S.; Ren, D.; Bolnykh, V.; et al. A universal co-solvent dilution strategy enables facile and cost-effective fabrication of perovskite photovoltaics. *Nat. Commun.* **2022**, *13*, 89. [CrossRef]

50. Yaghoobi Nia, N.; Giordano, F.; Zendehdel, M.; Cinà, L.; Palma, A.L.; Medaglia, P.G.; Zakeeruddin, S.M.; Grätzel, M.; Di Carlo, A. Solution-based heteroepitaxial growth of stable mixed cation/anion hybrid perovskite thin film under ambient condition via a scalable crystal engineering approach. *Nano Energy* **2020**, *69*, 104441. [CrossRef]

51. Teo, S.H.; Ng, C.H.; Ng, Y.H.; Islam, A.; Hayase, S.; Taufiq-Yap, Y.H. Resolve deep-rooted challenges of halide perovskite for sustainable energy development and environmental remediation. *Nano Energy* **2022**, *99*, 107401. [CrossRef]

52. Ochedi, F.O.; Liu, D.; Yu, J.; Hussain, A.; Liu, Y. Photocatalytic, electrocatalytic and photoelectrocatalytic conversion of carbon dioxide: A review. *Environ. Chem. Lett.* **2021**, *19*, 941–967. [CrossRef]

53. Mao, X.; Hatton, T.A. Recent Advances in Electrocatalytic Reduction of Carbon Dioxide Using Metal-Free Catalysts. *Ind. Eng. Chem. Res.* **2015**, *16*, 4033–4042. [CrossRef]

54. Kumaravel, V.; Bartlett, J.; Pillai, S.C. Photoelectrochemical Conversion of Carbon Dioxide (CO_2) into Fuels and Value-Added Products. *ACS Energy Lett.* **2020**, *5*, 486–519. [CrossRef]

55. Kim, J.; Jeong, S.; Beak, M.; Park, J.; Kwon, K. Performance of Photovoltaic-Driven Electrochemical Cell Systems for CO_2 Reduction. *Chem. Eng. J.* **2022**, *15*, 130259. [CrossRef]

56. Chen, K.; Qi, K.; Zhou, T.; Yang, T.; Zhang, Y.; Guo, Z.; Lim, C.K.; Zhang, J.; Žutic, I.; Zhang, H.; et al. Water-Dispersible $CsPbBr_3$ Perovskite Nanocrystals with Ultra-Stability and its Application in Electrochemical CO_2 Reduction. *Nano-Micro Lett.* **2021**, *13*, 172. [CrossRef] [PubMed]

57. Li, Y.; Chen, X.; Yang, Y.; Jiang, Y.; Xia, C. Mixed-Conductor $Sr_2Fe_{1.5}Mo_{0.5}O_{6-\delta}$ as Robust Fuel Electrode for Pure CO_2 Reduction in Solid Oxide Electrolysis Cell. ACS Sustain. *Chem. Eng.* **2017**, *5*, 11403–11412.

58. Pi, Y.; Guo, J.; Shao, Q.; Huang, X. All-inorganic $SrSnO_3$ perovskite nanowires for efficient CO_2 electroreduction. *Nano Energy* **2019**, *62*, 861–868. [CrossRef]

59. Hou, P.; Wang, X.; Wang, Z.; Kang, P. Gas Phase Electrolysis of Carbon Dioxide to Carbon Monoxide Using Nickel Nitride as the Carbon Enrichment Catalyst. *ACS Appl. Mater. Interfaces* **2018**, *10*, 38024–38031. [CrossRef]

60. Yin, Z.; Yu, C.; Zhao, Z.; Guo, X.; Shen, M.; Li, N.; Muzzio, M.; Li, J.; Liu, H.; Lin, H.; et al. Cu_3N nanocubes for selective electrochemical reduction of CO_2 to ethylene. *Nano Lett.* **2019**, *19*, 8658–8663. [CrossRef]

61. Hu, S.; Zhang, L.; Cai, L.; Cao, Z.; Jiang, Q.; Yu, W.; Wu, Y.; Zhu, X.; Yang, W. Iron stabilized 1/3 A-site deficient La–Ti–O perovskite cathodes for efficient CO_2 electroreduction. *J. Mater. Chem. A* **2020**, *8*, 21053–21061. [CrossRef]

62. Chen, S.; Su, Y.; Deng, P.; Qi, R.; Zhu, J.; Chen, J.; Wang, Z.; Zhou, L.; Guo, X.; Xia, B.Y. Highly Selective Carbon Dioxide Electroreduction on Structure-Evolved Copper Perovskite Oxide toward Methane Production. *ACS Catal.* **2020**, *10*, 4640–4646. [CrossRef]

63. Hu, S.; Zhang, L.; Liu, H.; Li, W.; Cao, Z.; Cai, L.; Zhu, Y.; Zhu, X.; Yang, W. Detrimental phase evolution triggered by Ni in perovskite-type cathodes for CO_2 electroreduction. *J. Energy Chem.* **2019**, *36*, 87–94. [CrossRef]

64. Ma, M.; Yang, X.; Xu, C.; Ren, R.; Qiao, J.; Sun, W.; Wang, Z.; Sun, K. Constructing highly active alloy-perovskite interfaces for efficient electrochemical CO_2 reduction reaction. *Sep. Purif. Technol.* **2022**, *296*, 121411. [CrossRef]

65. Wang, Y.; Wang, C.; Wei, Y.; Wei, F.; Kong, L.; Feng, J.; Lu, J.-Q.; Zhou, X.; Yang, F. Efficient and Selective Electroreduction of CO_2 to HCOOH over Bismuth-Based Bromide Perovskites in Acidic Electrolytes. *Chem. Eur. J.* **2022**, *28*, e202201832. [CrossRef] [PubMed]

66. Zhu, Y.; Zhou, W.; Dong, Z.; Zhang, X.; Chen, Z.; Liu, Z.; Li, F.; Fan, J.; Jiao, M.; Liu, L. Nanosized $LaInO_3$ perovskite for efficient electrocatalytic reduction of CO_2 to formate. *J. CO2 Util.* **2023**, *68*, 102342. [CrossRef]

67. Bae, K.T.; Jeong, I.; Akromjon, A.; Im, H.N.; Lee, K.T. Robust and efficient Fe/Mn bimetal doped $Pr4/3Ba2/3Co2/3Fe2/3Mn2/3O5+\delta$ double perovskite catalysts for direct CO_2 electrolysis. *Chem. Eng. J.* **2023**, *472*, 145015. [CrossRef]

68. Sivula, K.; Van De Krol, R. Semiconducting materials for photoelectrochemical energy conversion. *Nat. Rev. Mater.* **2016**, *1*, 15010. [CrossRef]

69. Sun, H.; Song, S.; Xu, X.; Dai, J.; Yu, J.; Zhou, W.; Shao, Z.; Jung, W. Recent Progress on Structurally Ordered Materials for Electrocatalysis. *Adv. Energy Mater.* **2021**, *11*, 2101937. [CrossRef]

70. Arandiyan, H.; Mofarah, S.S.; Sorrell, C.C.; Doustkhah, E.; Sajjadi, B.; Hao, D.; Wang, Y.; Sun, H.; Ni, B.J.; Rezaei, M.; et al. Defect engineering of oxide perovskites for catalysis and energy storage: Synthesis of chemistry and materials science. *Chem. Soc. Rev.* **2021**, *50*, 10116–10211. [CrossRef]

71. Chen, J.; Yin, J.; Zheng, X.; Ait Ahsaine, H.; Zhou, Y.; Dong, C.; Mohammed, O.F.; Takanabe, K.; Bakr, O.M. Compositionally Screened Eutectic Catalytic Coatings on Halide Perovskite Photocathodes for Photoassisted Selective CO_2 Reduction. *ACS Energy Lett.* **2019**, *4*, 1279–1286. [CrossRef]

72. Wang, Q.; Tao, L.; Jiang, X.; Wang, M.; Shen, Y. Graphene oxide wrapped $CH_3NH_3PbBr_3$ perovskite quantum dots hybrid for photoelectrochemical CO_2 reduction in organic solvents. *Appl. Surf. Sci.* **2019**, *465*, 607–613. [CrossRef]

73. Zhang, H.; Chen, Y.; Wang, H.; Wang, H.; Ma, W.; Zong, X.; Li, C. Carbon Encapsulation of Organic–Inorganic Hybrid Perovskite toward Efficient and Stable Photo-Electrochemical Carbon Dioxide Reduction. *Adv. Energy Mater.* **2020**, *10*, 2002105. [CrossRef]

74. Jang, Y.J.; Jeong, I.; Lee, J.; Lee, J.; Ko, M.J.; Lee, J.S. Unbiased Sunlight-Driven Artificial Photosynthesis of Carbon Monoxide from CO_2 Using a ZnTe-Based Photocathode and a Perovskite Solar Cell in Tandem. *ACS Nano.* **2016**, *10*, 6980–6987. [CrossRef]

75. Zhang, X.; Tang, R.; Sun, H.; Yang, W.; Liang, W.; Li, F.; Zheng, R.; Huang, J. Synergistically Interface-Engineered Inorganic Halide Perovskite Photocathodes for Photoelectrochemical CO_2 Reduction. *Energy Fuels* **2023**. [CrossRef]

76. Schreier, M.; Héroguel, F.; Steier, L.; Ahmad, S.; Luterbacher, J.S.; Mayer, M.T.; Luo, J.; Grätzel, M. Solar conversion of CO_2 to CO using Earth-abundant electrocatalysts prepared by atomic layer modification of CuO. *Nat. Energy* **2017**, *2*, 17087. [CrossRef]

77. Huan, T.N.; Dalla Corte, D.A.; Lamaison, S.; Karapinar, D.; Lutz, L.; Menguy, N.; Foldyna, M.; Turren-Cruz, S.H.; Hagfeldt, A.; Bella, F.; et al. Low-cost high-efficiency system for solar-driven conversion of CO_2 to hydrocarbons. *Proc. Natl. Acad. Sci. USA* **2019**, *116*, 9735–9740. [CrossRef] [PubMed]

78. Schreier, M.; Curvat, L.; Giordano, F.; Steier, L.; Abate, A.; Zakeeruddin, S.M.; Luo, J.; Mayer, M.T.; Grätzel, M. Efficient photosynthesis of carbon monoxide from CO_2 using perovskite photovoltaics. *Nat. Commun.* **2015**, *6*, 7326. [CrossRef] [PubMed]

79. Esiner, S.; Wang, J.; Janssen, R.A.J. Light-Driven Electrochemical Carbon Dioxide Reduction to Carbon Monoxide and Methane Using Perovskite Photovoltaics. *Cell Rep. Phys. Sci.* **2020**, *1*, 100058. [CrossRef]

80. Zhang, W.; Xia, Y.; Chen, S.; Hu, Y.; Yang, S.; Tie, Z.; Jin, Z. Single-Atom Metal Anchored Zr6-Cluster-Porphyrin Framework Hollow Nanocapsules with Ultrahigh Active-Center Density for Electrocatalytic CO_2 Reduction. *Nano Lett.* **2022**, *22*, 3340–3348. [CrossRef]

81. Khandy, S.A.; Islam, I.; Kaur, K.; Ali, A.M.; El-Rehim, A.F.A. Electronic structure, stability, photocatalytic and optical properties of new lead-free double perovskites Tl2PtX6 (X = Cl, Br) for light-harvesting applications. *Mater. Chem. Phys.* **2023**, *297*, 127293. [CrossRef]

82. Bhat, A.A.; Khandy, S.A.; Ali, A.M.; Tomar, R. Photoluminescence Emission Studies on a Lanthanum-Doped Lead Free Double Halide Perovskite, La:Cs2SnCl6. *J. Phys. Chem. Lett.* **2023**, *14*, 5004–5012. [CrossRef]

83. Zhang, M.; Jeerh, G.; Zou, P.; Lan, R.; Wang, M.; Wang, H.; Tao, S. Recent development of perovskiteoxide-based electrocatalysts and their applications in low to intermediate temperature electrochemical devices. *Mater. Today* **2021**, *49*, 351–377. [CrossRef]